Actin-dependent Propulsion of Endosomes and Lysosomes by Recruitment of N-WASP✪

Jack Taunton,* Brian A. Rowning,‡ Margaret L. Coughlin,* Michael Wu,§ Randall T. Moon,‖ Timothy J. Mitchison,* and Carolyn A. Larabell‡

*Department of Cell Biology, Harvard Medical School, Boston, Massachusetts 02115; ‡Lawrence Berkeley National Laboratory, Berkeley, California 94720; §Department of Molecular and Cell Biology, University of California Berkeley, Berkeley, California 94720; and ‖Howard Hughes Medical Institute, Department of Pharmacology, University of Washington School of Medicine, Seattle, Washington 98195

Abstract. We examined the spatial and temporal control of actin assembly in living *Xenopus* eggs. Within minutes of egg activation, dynamic actin-rich comet tails appeared on a subset of cytoplasmic vesicles that were enriched in protein kinase C (PKC), causing the vesicles to move through the cytoplasm. Actin comet tail formation in vivo was stimulated by the PKC activator phorbol myristate acetate (PMA), and this process could be reconstituted in a cell-free system. We used this system to define the characteristics that distinguish vesicles associated with actin comet tails from other vesicles in the extract. We found that the protein, N-WASP, was recruited to the surface of every vesicle associated with an actin comet tail, suggesting that vesicle movement results from actin assembly nucleated by the Arp2/3 complex, the immediate downstream target of N-WASP. The motile vesicles accumulated the dye acridine orange, a marker for endosomes and lysosomes. Furthermore, vesicles associated with actin comet tails had the morphological features of multivesicular endosomes as revealed by electron microscopy. Endosomes and lysosomes from mammalian cells preferentially nucleated actin assembly and moved in the *Xenopus* egg extract system. These results define endosomes and lysosomes as recruitment sites for the actin nucleation machinery and demonstrate that actin assembly contributes to organelle movement. Conversely, by nucleating actin assembly, intracellular membranes may contribute to the dynamic organization of the actin cytoskeleton.

Key words: actin assembly • fertilization • Wiskott-Aldrich • phorbol ester • Rho-GDI

Introduction

The spatial arrangement of cytoplasmic organelles is coordinated by dynamic interactions with microtubules and actin filaments. There is substantial biochemical, cytological, and genetic evidence to support a mechanism in which molecular motors couple the energy of ATP hydrolysis to the directed transport of membrane vesicles along tracks formed by cytoskeletal polymers (Goodson et al., 1997). However, for most membrane compartments, the precise mechanisms specifying their positions within the cell and their interactions with microtubules and actin have not been delineated. In many regions of the cytoplasm, microtubules and actin filaments are not stable tracks but are instead dynamic polymers undergoing continual assembly and disassembly. The implications of cytoskeletal polymer dynamics for organelle movement have been little emphasized.

The pathogenic bacterium, *Listeria monocytogenes*, uses a distinct mechanism to generate the force required for movement that apparently does not involve molecular motors (Loisel et al., 1999). *Listeria* propels itself through the cytoplasm of a mammalian host cell by nucleating actin filament assembly on the surface of its outer membrane. Newly assembled actin filaments are cross-linked to form a dense comet tail structure that undergoes rapid disassembly by cytoplasmic actin depolymerizing factors. *Shigella*, *Rickettsia*, and vaccinia virus have been shown to exploit similar motility mechanisms (Higley and Way, 1997). Have these unrelated pathogens evolved a unique mechanism for intracellular movement, or have they appropri-

✪The online version of this article contains supplemental material.

Address correspondence to Jack Taunton, Harvard Medical School, Department of Cell Biology, 240 Longwood Ave., Boston, MA 02115. Tel.: (617) 432-3804. Fax: (617) 432-3702. E-mail: jack_taunton@hms.harvard.edu

ated a mechanism normally employed by their host for the movement of its organelles?

Although described as a model system for actin dynamics at the plasma membrane of a migrating cell, *Listeria* more closely resembles a cellular organelle in terms of its size and shape. During the course of studies on *Listeria* movement in crude *Xenopus* egg extracts, we and others occasionally observed actin-rich comet tails in the absence of added *Listeria* (T.J. Mitchison, unpublished observations; Marchand et al., 1995). Two recent studies found that this phenomenon could be potentiated by GTPγS and orthovanadate, and through the use of dominant mutant constructs, demonstrated a requirement for the Rho family GTPase Cdc42 (Ma et al., 1998; Moreau and Way, 1998). These studies did not address whether actin-dependent vesicle movement occurs in vivo, nor did they characterize the motile vesicles. We were thus inspired to address three questions. First, do vesicles move by a *Listeria*-like mechanism in living *Xenopus* eggs? Second, how do vesicles signal the recruitment and activation of the cytosolic actin nucleation machinery? Third, what features distinguish the vesicles that nucleate actin assembly from those that do not?

We chose to examine *Xenopus* eggs immediately after fertilization because we suspected that second messengers produced at fertilization might be responsible for signaling to cytosolic actin nucleation factors. Sperm entry causes rapid elevation of intracellular calcium and diacylglycerol, the endogenous activators of conventional protein kinase C (PKC)[1] isoforms, and these changes temporally coincide with the association of PKC with the membrane fraction (Stith et al., 1997). Moreover, the potent diacylglycerol mimetic, PMA, recapitulates the major cortical events of fertilization, including granule exocytosis, resumption of membrane trafficking, contraction of the cortex, and cleavage furrow formation (Bement and Capco, 1989, 1991). We therefore investigated the dynamic behavior of *Xenopus* PKCα (a conventional PKC isoform) fused to green fluorescent protein (XPKCα-GFP) along with rhodamine-labeled actin during egg activation. We discovered that XPKCα-GFP localized to cytoplasmic vesicles. A subset of these vesicles nucleated actin assembly and moved in a manner reminiscent of *Listeria*. PMA powerfully stimulated actin assembly-dependent vesicle movement in vivo and in a cell-free system, and we have used this system to further characterize the motile vesicles.

Materials and Methods

Live Cell Imaging

Xenopus PKCα (Chen et al., 1988), was cloned upstream of enhanced GFP (Heim et al., 1995), in the *Xenopus* expression vector CS2+. The resulting fusion protein, XPKCα-GFP, is enzymatically active in vitro and in cultured cells is recruited to the plasma membrane in response to PMA (Sheldahl et al., 1999). Approximately 5 nl of XPKCα-GFP RNA and 20 nl of a stock solution of rhodamine-labeled non-muscle actin (10 mg/ml in 2 mM Tris-HCl [pH 8.0], 0.2 mM $CaCl_2$, 0.2 mM ATP, and 0.5 mM DTT; Cytoskeleton) were injected into manually defolliculated stage VI oocytes. After 8–10 h, meiotic maturation was triggered by the addition of 1 μg/ml progesterone, and oocytes were incubated overnight in Barth's medium at 16–17°C. Several hours after germinal vesicle breakdown, oocytes were activated by pricking with a glass micropipet. Oocytes were mounted in viewing dishes for live cell analyses as described previously (Rowning et al., 1997; Larabell, 1998), using a BioRad MRC 1024 confocal laser scanning microscope equipped with a Nikon Diaphot 200 microscope and a Nikon 60× PlanApo 1.4 NA oil immersion lens. XPKCα-GFP constructs and rhodamine-actin were visualized using fluorescein and rhodamine filters, respectively. Optical sections from the outer 20 μm were collected. For a given time-lapse sequence, multiple images of a single optical section were collected as rapidly as possible. Images were collected using a 512 × 512-pixel format at 1 frame per 3.5 s for up to 1 h. Data were analyzed using ImageSpace software (Molecular Dynamics) on a Silicon Graphics computer.

Whole Mount Immunocytochemistry

Eggs were collected from adult frogs and fertilized as described previously (Rowning et al., 1997). They were fixed overnight in 4% paraformaldehyde, 0.1% glutaraldehyde, 100 mM KCl, 3 mM $MgCl_2$, 10 mM Hepes, 150 mM sucrose, and 0.1% Triton X-100 (pH 7.6). Nonspecific binding was blocked by incubation (1–2 h, with rotation) in 0.1% Triton X-100 in Super Block (Pierce). Specimens were then incubated for 1 h with 0.16 μM fluorescein-phalloidin in Super Block. Eggs were viewed with a BioRad 1024 confocal laser scanning microscope using a fluorescein filter.

Cell-free Reconstitution of Vesicle Movement

Crude *Xenopus* egg extract was prepared as described except that cytochalasin D was omitted (Murray and Kirschner, 1989). Cytosol and a heavy membrane fraction were prepared by centrifugation of the crude extract (2 h, 300,000 *g* max; Beckman SW-50 rotor). The viscous glycogen pellet beneath the membrane layer was discarded. Cytosol was further clarified by spinning for 15 min at 541,000 *g* max (Beckamn TLA 100.3 rotor). Crude membranes (diluted with one volume of 2 M sucrose) and cytosol were snap frozen in separate aliquots for storage at –80°C unless otherwise indicated. Clarified cytosol contained a small population of vesicles, but motility assays were far more robust (more comet tails over a longer time period) when cytosol was supplemented with the heavy membrane fraction.

For the standard assay, crude membranes in 1 M sucrose (20-μl aliquot, derived from ~80 μl crude extract) were washed and resuspended in 14 μl buffer A (50 mM NaCl, 5 mM $MgCl_2$, and 50 mM tris [pH 7.5]). To the membrane suspension were added 35 μl cytosol (derived from ~80 μl crude extract), 0.3 μl rhodamine-labeled actin (Kellogg et al., 1988), 3 μl PMA (20 μM stock in 10% DMSO), and 20 μl buffer A at 4°C. 20-μl samples were then warmed to room temperature. After 30–40 min, 2-μl aliquots were viewed with a Nikon E800 microscope. Images were acquired with a Princeton Instruments cooled CCD camera (standard rhodamine filter set) and analyzed with Winview or Metamorph software. Pixels having an intensity over a threshold value (set to a value greater than the background fluorescence in regions devoid of comet tails) were summed over 10 random fields to quantitate relative actin assembly.

In the experiment presented in Fig. 5, rhodamine-actin was replaced by acridine orange (20 μg/ml) and freshly prepared extracts were used. Images were acquired using phase contrast optics and a Texas red filter set, and comet tails were scored for colocalization of red fluorescence (three experiments, $n = 417$ comet tails).

Immunofluorescence Microscopy

Vesicle motility reactions were perfused into 10-μl chambers composed of a glass microscope slide, double-sided tape, and a poly-lysine coated Aclar coverslip (Ted Pella, Inc.). Some reactions contained 1 μg/ml *Clostridium difficile* ToxB (prepared as a GST fusion protein as described; Hofmann et al., 1997). After 30 min, reactions were fixed by gently perfusing with 4% paraformaldehyde in cytoskeleton buffer (10 mM MES, pH 6.1, 138 mM KCl, 3 mM $MgCl_2$, 2 mM EGTA, and 0.32 M sucrose) for 20 min. Reactions containing Texas red transferrin–labeled membranes were fixed with 4% paraformaldehyde/0.1% glutaraldehyde. The perfusion chambers were washed with TBS and blocked with 2% BSA/TBS (for Sec61β and Lamp-1 immunolabeling, all solutions after the fixation step contained 0.2 mg/ml saponin). Primary antibodies (1-h incubation) were diluted into 2% BSA/TBS as follows: affinity-purified rabbit anti–N-WASP, 1:1000 (Ro-

[1]*Abbreviations used in this paper:* BIM-I, bisindolylmaleimide I; GDI, guanine-nucleotide dissociation inhibitor; GFP, green fluorescent protein; PKC, protein kinase C; PNS, postnuclear supernatant.

hatgi et al., 1999); affinity-purified rabbit anti-Sec61β, 1:100 (Gorlich et al., 1992); H4A3 mouse anti–Lamp-1 hybridoma supernatant, 1:5 (Developmental Studies Hybridoma Bank). Texas red–labeled secondary antibodies (Jackson Laboratories) were diluted 1:100 (1-h incubation), and FITC-phalloidin (20 min incubation; Sigma) was diluted to 1 μg/ml. Chambers were perfused with mounting media (60% glycerol/TBS/0.5% *p*-phenylenediamine), sealed with VALAP, and viewed with a 60× objective on a Nikon E600 epifluorescence microscope mounted with a Princeton Instruments cooled CCD camera.

Electron Microscopy

Vesicle motility reactions with freshly prepared *Xenopus* cytosol and membranes (described above) were perfused into 10-μl chambers composed of a glass microscope slide, double-sided tape, and a poly-lysine–coated Aclar coverslip (Ted Pella, Inc.). Samples were fixed by perfusing with 50 mM lysine/3% glutaraldehyde in 0.1 M cacodylate buffer (pH 7.0) for 10 min, followed by 3% glutaraldehyde in cacodylate buffer for 20 min (Boyles et al., 1985). Samples were post-fixed with osmium, stained with 2% uranyl acetate, dehydrated, and embedded with Epon aryldite. Small pieces of embedded sample were excised, mounted, and sectioned (55-nm sections). Sections were stained with 2% uranyl acetate in 50% methanol, then 0.4% lead citrate, and viewed on a JEOL 1200 EX microscope.

For immunogold labeling, perfusion chamber reactions containing membrane-free *Xenopus* cytosol and HeLa membranes were fixed with 4% paraformaldehyde for 20 min and immunolabeled exactly as described above for immunofluorescence except that 15-nm protein A–gold (J.W. Slot) was used instead of the secondary antibody (1:50 dilution). After immunolabeling, the samples were fixed with lysine/glutaraldehyde and processed for electron microscopy exactly as described above.

Preparation and Motility Assay of Mammalian Cell Endosomes

HeLa cells were cultured in DME with 10% fetal calf serum. Cells (2 × 15-cm dishes, ~90% confluent) were cultured for 30 min in serum-free media containing 2 mg/ml BSA. Cells were then labeled for 20 min at 4°C or 37°C with 40 μg/ml Texas red transferrin (Molecular Probes), washed three times with cold PBS, and scraped into PBS. Cells were washed once with lysis buffer (0.25 M sucrose, 20 mM Hepes, pH 7.7) and then resuspended in 2 vol of lysis buffer with protease inhibitors (10 μg/ml leupeptin, pepstatin, and chymostatin and 0.2 mM phenylmethanesulfonyl fluoride). They were lysed by passage through a 27-gauge needle (5–7 times; cell breakage was monitored by phase contrast microscopy). Centrifugation for 10 min at 5,000 *g* max provided the postnuclear supernatant (PNS). For immunofluorescence experiments in perfusion chambers, the PNS from an equal number of unlabeled cells was prepared in parallel. For all motility assays with HeLa membranes, the PNS was diluted 60-fold into membrane-free *Xenopus* cytosol (see below) containing 1 μM PMA. For the time-lapse experiments, 0.5 μM Alexa (488)–labeled actin (Molecular Probes) was included. A 2.5-μl aliquot of the cell-free motility reaction was placed on a glass slide under a coverslip and sealed with VALAP. Texas red and fluorescein images were acquired every 10 s using Metamorph software to drive a filter wheel and an automatic shutter mounted on a Nikon E600 upright microscope.

Membrane-free *Xenopus* cytosol was prepared as follows: freshly prepared cytosol (2 ml) was diluted with 12.5 ml buffer A and 0.68 ml ATP-regenerating mix (20 mM ATP, 20 mM $MgCl_2$, and 150 mM creatine phosphate) and centrifuged for 1 h at 450,000 *g* max. The supernatant (12 ml) was concentrated with a Centriprep 10 concentrator (Millipore) to a final volume of 2 ml.

Online Supplemental Material

Video 1. Actin comet tail formation in an activated *Xenopus* egg as depicted in Fig. 1 D. Rhodamine-actin comet tails form at PKC-GFP encircled vesicles in the egg periphery during the first 15–20 min after activation. The actin comet tails effect vesicle displacement at ~10 μm/min. In vivo time-lapse sequence collected with a confocal microscope at 3.5-s intervals.

Video 2. Actin comet tail formation in an egg activated with PMA as depicted in Fig. 2 B. Actin comet tails are more abundant and persist for longer times (1 h) in response to PMA activation (compare with egg in Video 1). In vivo time-lapse sequence collected with a confocal microscope at 3.5-s intervals.

Videos available at http://www.jcb.org/cgi/content/full/148/3/519/DC1.

Results

Protein Kinase C and Actin Dynamics during Xenopus Egg Activation

We considered that simultaneous observation of PKC and actin dynamics during *Xenopus* egg activation might reveal specialized domains of regulated actin assembly. To this end, we injected *Xenopus* oocytes with rhodamine-actin and RNA encoding XPKCα-GFP and treated them with progesterone to induce maturation. Examination of the cortical cytoplasm of mature eggs by confocal microscopy revealed diffuse fluorescence of both actin and XPKCα-GFP (Fig. 1 A). We activated the eggs by pricking them with a glass micropipet in a calcium-containing buffer, an established model for fertilization. Within 4 min of activation, we observed a dramatic accumulation of XPKCα-GFP on the surface of previously undetectable vesicles; a subset of these vesicles colocalized with bright puncta of rhodamine actin (Fig. 1 B). Diacylglycerol production and PKC activation are well-characterized responses to *Xenopus* egg activation (Stith et al., 1997), but localization of PKC to cytoplasmic vesicles has not been observed previously in *Xenopus* eggs.

At 3–5 min after activation, the cortex began to contract. After the peak of cortical contraction, a subpopulation of the XPKCα-GFP labeled vesicles developed dynamic actin-rich comet tails and were propelled through the cytoplasm (Figs. 1, C and D). We observed actin comet tails behind moving vesicles in 18 out of 18 time-lapse experiments. Moving vesicles persisted within a single focal plane for 5–10 min, with some comet tails visible for up to 20 min. Tracking individual comet tails that remained in a single focal plane revealed a mean velocity of 10.4 ± 1.1 μm/min ($n = 9$).

We next asked whether actin comet tails form in fertilized eggs. Eggs were fixed as soon as possible after fertilization (~8 min were required to remove the jelly coats) and at various time points thereafter, then prepared for observation by whole mount immunocytochemistry. Those eggs fixed 8–15 min after fertilization displayed actin-rich comet tails throughout the periphery as seen by fluorescein-phalloidin staining (Fig. 2 A, $n = 37$). Unfertilized eggs ($n = 35$) and eggs fixed between 18 and 40 min after fertilization ($n = 35$) were devoid of comet tails (data not shown). Therefore, the appearance of comet tails occurs with a similar time course in fertilized and pricked eggs.

To test whether diacylglycerol plays a causal role in this process, we treated progesterone-matured eggs with PMA and monitored rhodamine-actin dynamics. PMA induced greater numbers of comet tails relative to fertilized or prick-activated eggs (Fig. 2 B), and they were observed over a much longer time period (at least 1 h), consistent with the greater metabolic stability of PMA relative to diacylglycerol. PMA thus provided a means of inducing actin comet tails without having to prick or fertilize the eggs. Given the rapid contraction of the cortex that occurs during fertilization and the likely involvement of actin in many aspects of this transformation, we felt that a cell-free

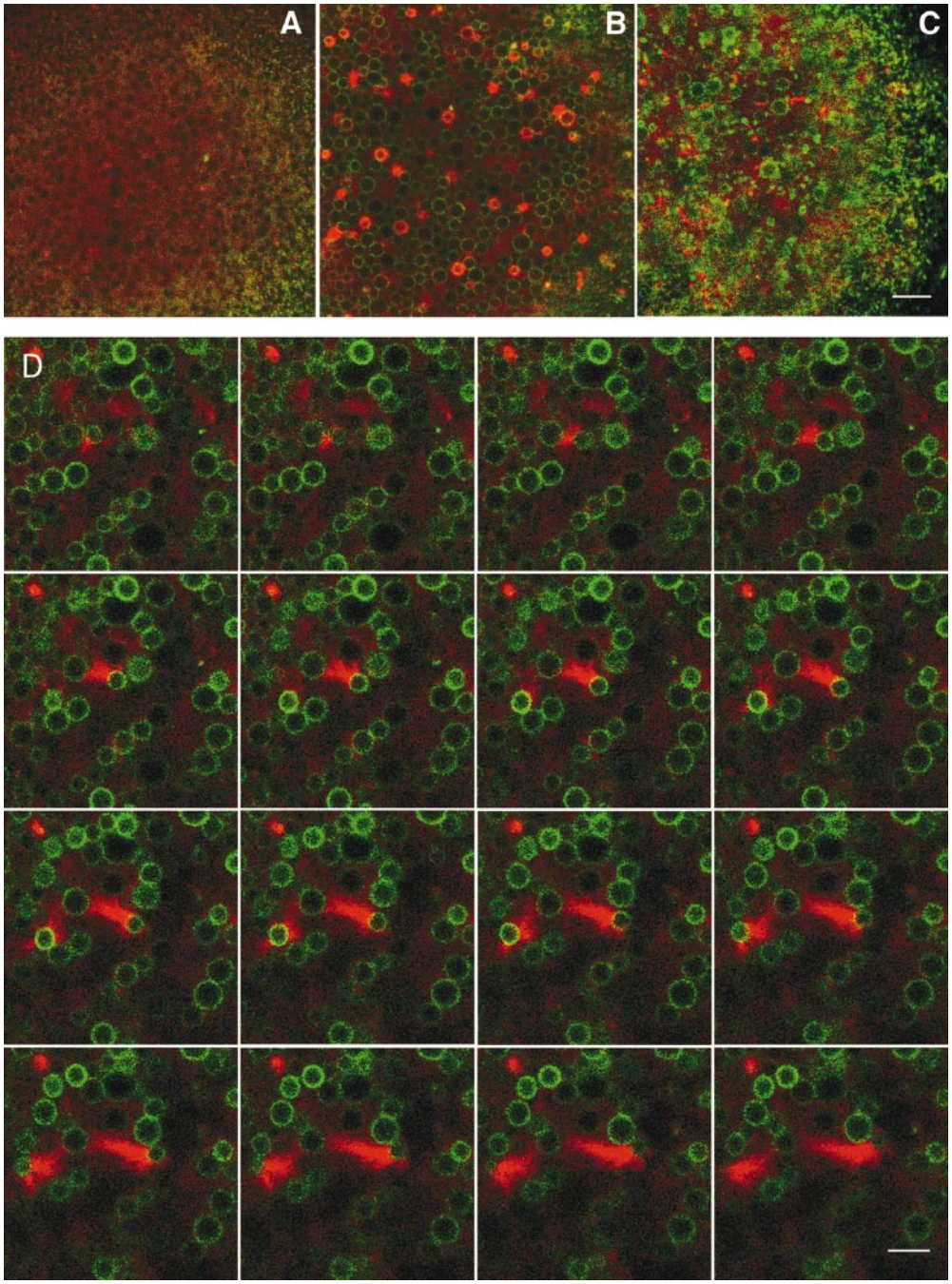

Figure 1. Actin comet tail formation in an activated *Xenopus* egg. (A) Vegetal pole of an egg, 2 min after activating the animal hemisphere by pricking with a glass micropipet. This region of the egg, viewed with a scanning laser confocal microscope, has not yet undergone activation-induced modifications. A diffuse distribution of rhodamine-actin and XPKCα-GFP is seen amidst the secretory cortical granules (1–3-μm-diam circular shadows) just beneath the plasma membrane. (B) Same region of the egg, 4 min after activation. The cortical secretory granules have undergone exocytosis and larger vesicles enriched in XPKCα-GFP (3–5-μm-diam) are now visible. As the egg reaches maximal contraction, large spherical accumulations of rhodamine-actin form amidst the field of vesicles. (C) A similar region of the egg after contraction (8 min after activation) showing numerous rhodamine-actin comet tails in a field of XPKCα-GFP vesicles of varying sizes. This is a tangential optical section, with the far right edge of the image showing microvillar tips on the egg surface and deeper regions of the egg cortex revealed on the left. (D) Time-lapse sequence (3.5-s intervals) showing the birth of rhodamine-actin comet tails. Actin assembly appears to be initiated by a PKC-enriched vesicle and ultimately effects a 10-μm displacement of that vesicle. See Online Supplemental Material, Video 1 (http://www.jcb.org/cgi/content/full/148/3/519/DC1). Bars: (A–C) 10 μm; (D) 5 μm.

system based on PMA stimulation would provide a more tractable starting point for mechanistic studies that focused specifically on actin-dependent vesicle propulsion.

Cell-free Reconstitution of PMA-Stimulated Actin Assembly and Vesicle Movement

We developed a cell-free system in *Xenopus* egg extracts that reconstitutes PMA-stimulated actin assembly on the surface of endogenous vesicles. Our system is similar to those used in previous studies (Ma et al., 1998; Moreau and Way, 1998), except that cytosol and a crude membrane fraction were separated so that they could be manipulated independently. Membranes were used in the following experiments at their approximate physiological concentrations.

Treatment of a mixture of cytosol (containing 0.5 μM rhodamine-actin) and the crude membrane fraction with 1 μM PMA resulted within 10 min in the assembly of dynamic actin-rich comet tails on a subset of the vesicles (Fig. 3 A). The 4α-stereoisomer of PMA, which fails to activate PKC, had no effect (data not shown). Actin assem-

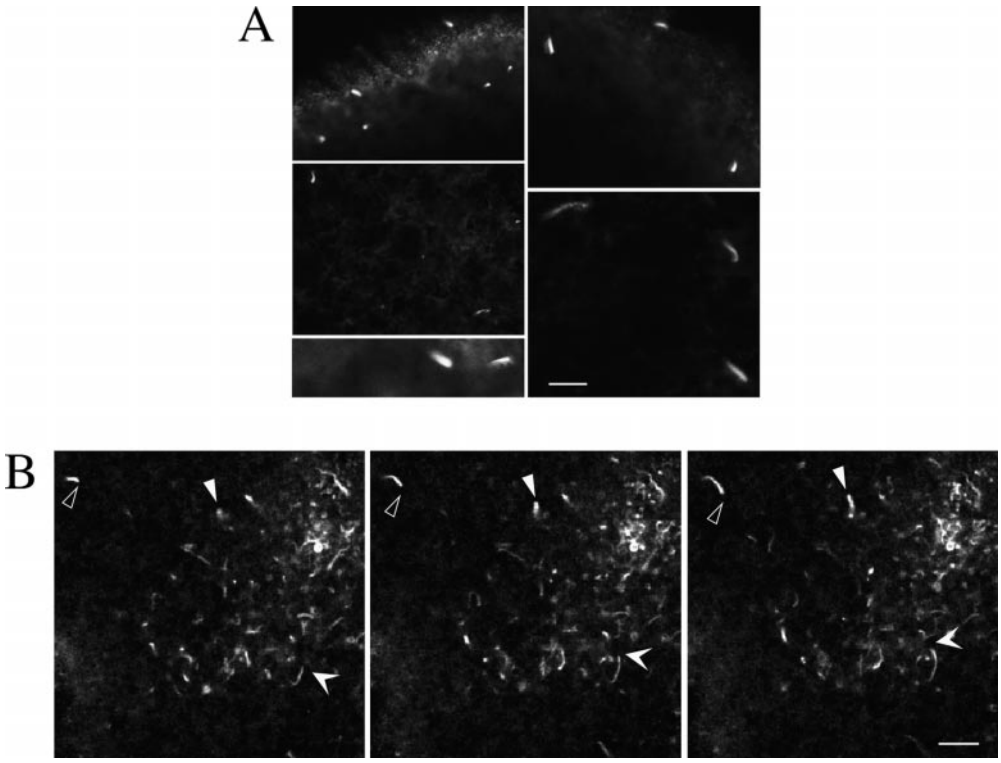

Figure 2. Comet tail formation in vivo induced by fertilization and PMA treatment. (A) Gallery of confocal images showing actin comet tails in eggs fixed 8 min after fertilization. F-actin was visualized by fluorescein-phalloidin staining. (B) In vivo time-lapse sequence (16-s intervals) showing rhodamine-actin comet tails (indicated by arrowheads) 20 min after treatment with 2 μM PMA. See Online Supplemental Material, Video 2 (http://www.jcb.org/cgi/content/full/148/3/519/DC1). Bars, 10 μm.

bly occurred specifically on the surface of vesicles as observed by epifluorescence and phase contrast microscopy (Fig. 3 A), resulting in movement at a rate of 8.2 ± 2.7 μm/min (n = 11), similar to the rate observed in vivo.

Fig. 3 B shows representative low magnification images from an experiment similar to that shown in Fig. 3 A. Cytosol, membranes, and rhodamine-actin were treated with 0.5% DMSO (control) or PMA, both alone and in the presence of the PKC active site inhibitor bisindolyl maleimide-I (BIM-I; Toullec et al., 1991). We quantitated the relative actin assembly activity by acquiring digital fluorescence images of 10 random fields and summing the total number of fluorescent pixels that were brighter than the background (Fig. 3 C). In the absence of PMA, actin comet tails were rarely detected (~1 comet tail per 10 fields), whereas PMA induced hundreds of comet tails per field (Fig. 3 B). PMA-stimulated comet tail formation was largely suppressed by BIM-I (Figs. 3, B and C), suggesting further that PKC regulates comet tail formation. The resemblance to moving *Listeria* and response to PMA suggest that the cell-free system recapitulates the vesicle movement phenomenon observed in vivo.

Recruitment of N-WASP to the Surface of Motile Vesicles

We suspected that a Rho family GTPase was required to recruit and/or activate a soluble actin nucleator on the surface of vesicles. Two well-characterized Rho GTPase inhibitors, RhoGDI and ToxB, abolished PMA-stimulated actin comet tail formation (data not shown), consistent with previous studies which used GTPγS and orthovanadate to induce actin comets in *Xenopus* egg extracts (Ma et al., 1998; Moreau and Way, 1998). We took advantage of the irreversible inhibitory properties of ToxB to identify the relevant Rho GTPase in our system. In work to be published elsewhere, we purified a soluble factor capable of rescuing ToxB-inactivated cytosol. The factor consisted of two polypeptides that were identified as the Rho GTPase Cdc42 and its regulatory subunit, RhoGDI. This finding confirms and extends previous work in which dominant mutant versions of Cdc42 were used to inhibit or stimulate actin assembly in *Xenopus* egg extracts (Ma et al., 1998; Moreau and Way, 1998). The mechanism by which Cdc42 stimulates actin assembly has recently been shown to involve a minimum of two additional components: N-WASP, a multidomain protein with which GTP-bound Cdc42 directly interacts, and the Arp2/3 complex, whose actin nucleation activity is stimulated by the COOH-terminal domain of N-WASP (Egile et al., 1999; Rohatgi et al., 1999).

To test whether N-WASP is recruited specifically to motile vesicles, we developed a perfusion chamber assay in which the membranes were fixed to the surface of a coverslip and analyzed by indirect immunofluorescence (Fig. 4; see Fig. 6 for characterization of the membranes by electron microscopy). Chambers containing a mixture of cytosol, crude membranes, and 1 μM PMA were gently perfused with 4% paraformaldehyde and fixed for 20 min. F-actin structures were visualized with FITC-phalloidin. Indirect immunofluorescence with an affinity-purified antibody against N-WASP (Rohatgi et al., 1999) revealed intense staining at the membrane-proximal ends of actin comet tails (100% colocalization, n = 524; Fig. 4). As expected from previous studies with *Listeria* and *Shigella*, components of the Arp2/3 complex localized throughout the actin comet tails (data not shown).

We performed two additional experiments to determine the extent to which N-WASP recruitment correlated with actin comet formation. When PMA was added in the pres-

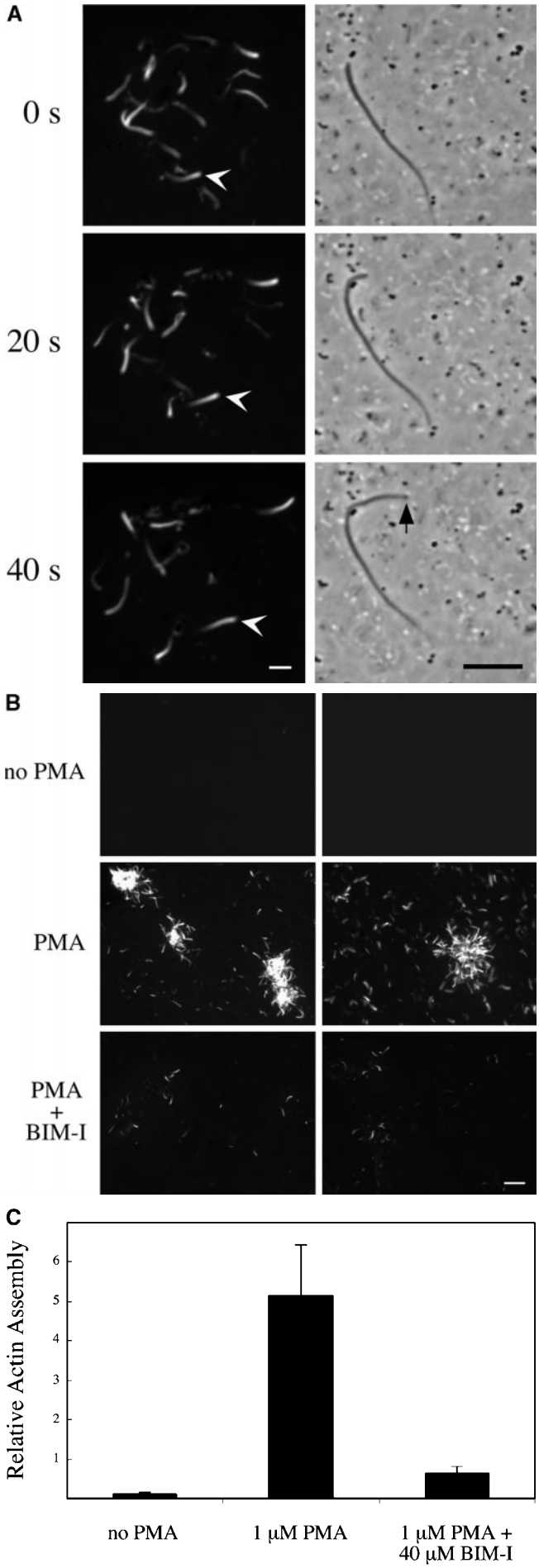

ence of 75 μM latrunculin A, an actin monomer sequestering compound, actin comet tails were not observed. However, intense N-WASP staining of a subset of the vesicles persisted under these conditions (Fig. 4). Thus, N-WASP recruitment can be experimentally uncoupled from vesicle propulsion. Remarkably, a faint ring of F-actin colocalized with N-WASP under these conditions, suggesting that when N-WASP is recruited to the membrane surface, it effectively competes with latrunculin to stabilize F-actin. N-WASP has been shown to bind to F-actin in solution, particularly in the presence of allosteric activators (Egile et al., 1999). Neither N-WASP nor actin was recruited to the membranes in the presence of ToxB (Fig. 4), consistent with the idea that recruitment and activation of N-WASP is mediated by Cdc42. Finally, N-WASP recruitment was rarely observed in the absence of PMA stimulation (1–5 puncta per coverslip; data not shown), and in every case N-WASP staining colocalized with an actin comet tail.

Motile Vesicles Have the Characteristics of Endosomes

We wished to determine whether the motile vesicles, which appeared to be a small subset of the organelles visible by phase contrast microscopy, could be classified according to functional and morphological criteria. First, we incubated vesicle motility reactions with acridine orange, a marker for endosomes and lysosomes (Matteoni and Kreis, 1987), and acquired fluorescence and phase contrast images of the live (unfixed) reactions. Of the vesicles associated with phase dense tails, 80% exhibited bright red fluorescence when viewed with a Texas red filter set ($n = 417$ actin comet tails, Fig. 5). Acridine orange labeling was abolished by the vacuolar proton pump inhibitors bafilomycin A and concanamycin A (data not shown), suggesting that the majority of the motile vesicles are endosomes and/or lysosomes.

Using the flow chambers described in Fig. 4, we developed a method for examining the ultrastructure of motile vesicles by thin-section electron microscopy. Dense comet tail structures were observed, and each was attached to a single, well-defined vesicle (Fig. 6). Unexpectedly, the majority of the vesicle profiles associated with comet tails (76%, $n = 115$ comet tails) contained smaller vesicles,

Figure 3. Reconstitution of PMA-stimulated actin assembly in vitro. (A) Time-lapse sequences showing actin comet tails in *Xenopus* egg extracts. Cytosol was supplemented with a crude membrane fraction, rhodamine-actin, and 1 μM PMA. After incubating at room temperature for 20 min, samples were viewed by fluorescence (left) or phase contrast (right; note higher magnification) microscopy. Arrowheads (left) indicate a moving comet tail. Arrow (bottom right) indicates a phase dense particle at the tip of the comet tail. (B) In vitro actin assembly reactions as in (A) performed in the presence or absence of the PKC inhibitor, BIM-I (40 μM). Fluorescence images from a control reaction without PMA are also presented. Low magnification (20× objective) images were acquired from ten random fields, two of which are depicted for each condition. (C) Quantitation of data presented in B. The total number of pixels with fluorescence intensities above the background were summed over 10 random fields. Data (mean ± SD) from three experiments are presented. Bars: (A) 10 μm; (B) 20 μm.

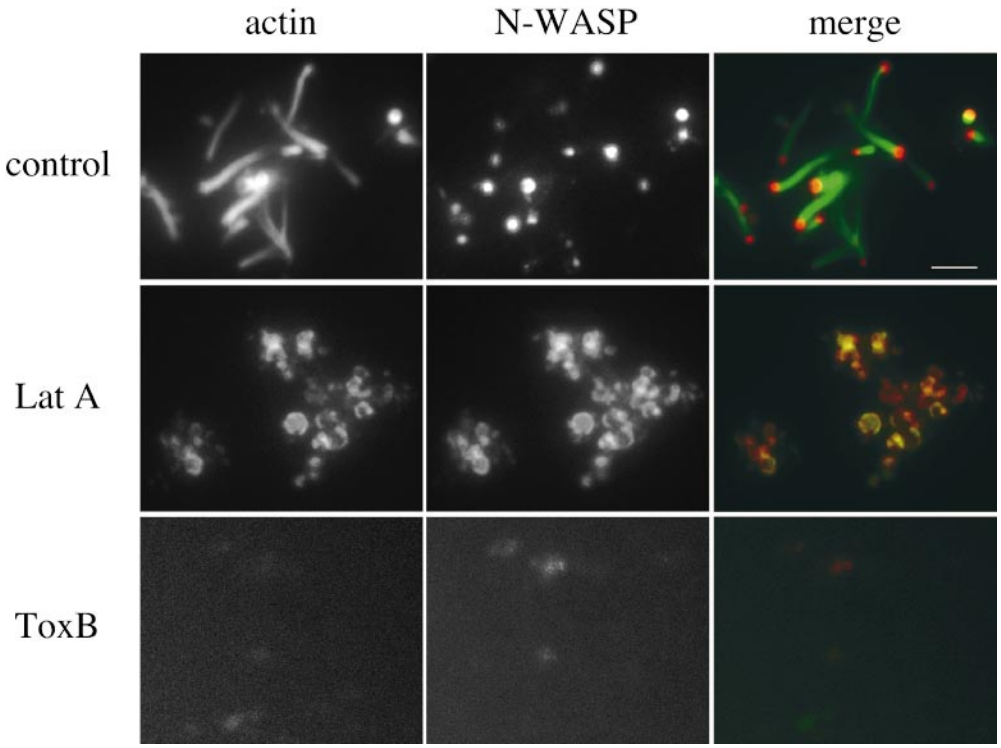

Figure 4. PMA stimulates the recruitment of N-WASP to vesicles associated with actin comet tails. Cell-free vesicle motility assays containing *Xenopus* cytosol, membranes, and 1 μM PMA were fixed in perfusion chambers and immunolabeled with affinity-purified anti–N-WASP antibodies followed by Texas red secondary antibodies and FITC-phalloidin. N-WASP and F-actin recruitment occurred in the presence of 75 μM latrunculin A, but comet tails were not observed. ToxB treatment prevented both N-WASP and F-actin recruitment, although nonspecific labeling of fixed membranes could be observed with long exposure times. Bar, 5 μm.

20–100 nm in diameter, within their limiting membranes (Fig. 6). This percentage is likely an underestimate because apparently empty vesicles may have contained internal vesicles in an adjacent section plane. Similar multivesicular bodies were identified previously in *Xenopus* oocytes and were shown to be specialized endosomes involved in vitellogenin processing (Wall and Patel, 1987).

Most of the vesicles associated with actin tails had highly irregular, nonspherical shapes, often with protrusions or invaginations (69%, $n = 115$). Circular profiles lacking internal vesicles were abundant in the extract but were never observed in association with comet tails. Finally, none of the 329 mitochondria identified had comet tails. These data suggest that, at least in the *Xenopus* extract system, vesicles having the stereotyped morphology of multivesicular endosomes are the preferential mediators of actin assembly.

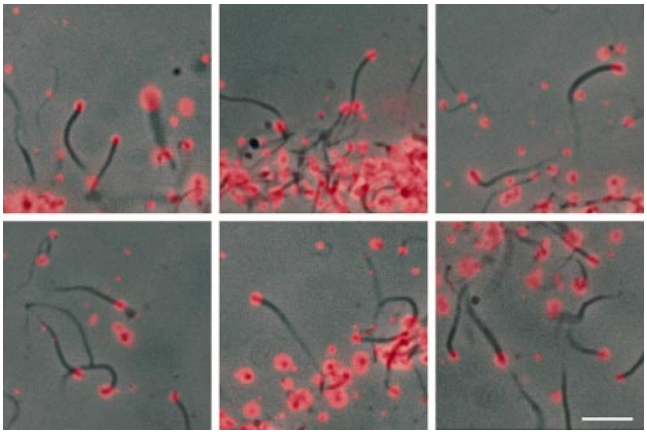

Figure 5. Accumulation of acridine orange, a marker for endosomes and lysosomes, in motile vesicles. Cell-free reactions (without rhodamine-actin) were monitored by phase contrast and fluorescence microscopy in the presence of 20 μg/ml acridine orange. A gallery of merged images (phase contrast and Texas red filter set) from three experiments is presented. 80% of the vesicles associated with comet tails strongly accumulated acridine orange ($n = 417$ comet tails). Bar, 10 μm.

Endosomes and Lysosomes from Mammalian Cells Preferentially Nucleate Actin Assembly In Vitro

The endocytic compartments of *Xenopus* eggs have not been well characterized. To test whether bona fide endosomes from other cell types promote actin assembly in our cell-free system, HeLa cells were allowed to internalize Texas red transferrin and a postnuclear supernatant (PNS) was prepared. The PNS was diluted 60-fold into membrane-free *Xenopus* cytosol containing 1 μM PMA and Alexa(488)-labeled actin. The time-lapse series depicted in Fig. 7 demonstrates that exogenous transferrin-positive endosomes formed actin comet tails and moved in a manner indistinguishable from the *Xenopus* egg vesicles. Thus, endosomes from cultured human cells are competent to undergo actin-dependent propulsion.

We noted that approximately half of the actin comet tails observed in the preceding experiment were not associated with labeled endosomes. We therefore wished to define further the nature of the vesicles that nucleate actin assembly and if possible, those that do not. Because there are few well-characterized molecular markers for *Xenopus* organelles, we focused on the HeLa membranes. Crude membranes were added to *Xenopus* cytosol to allow the different vesicle subpopulations to compete for essential signaling and actin nucleation components. Fig. 8 A shows

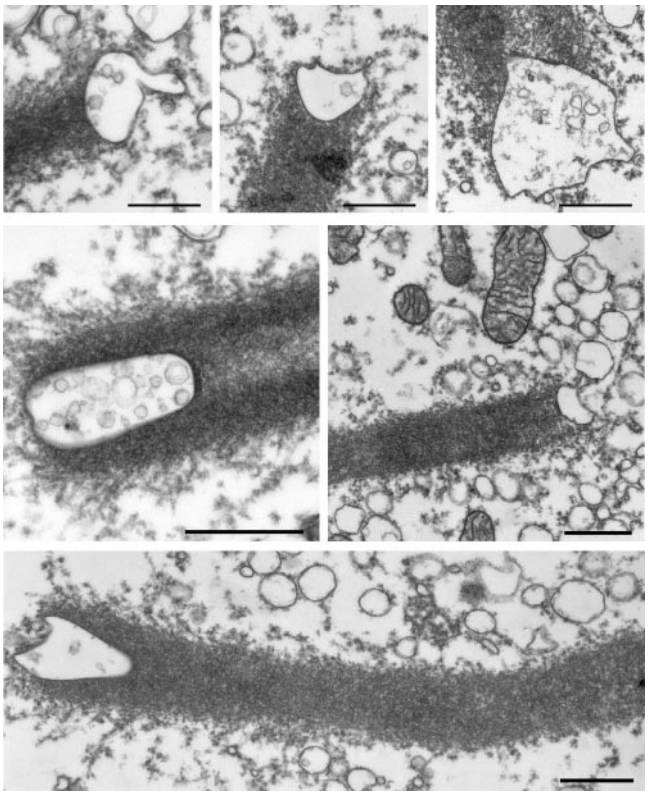

Figure 6. Thin-section electron microscopy analysis of vesicles associated with comet tails. Cell-free reactions were fixed in perfusion chambers and processed for electron microscopy (see Materials and Methods). A gallery of representative images was assembled to highlight the odd shapes, tubular processes, and multivesicular lumens of vesicles associated with tails. Note the clear circular profiles and mitochondria, none of which are associated with comet tails. Bars, 500 nm.

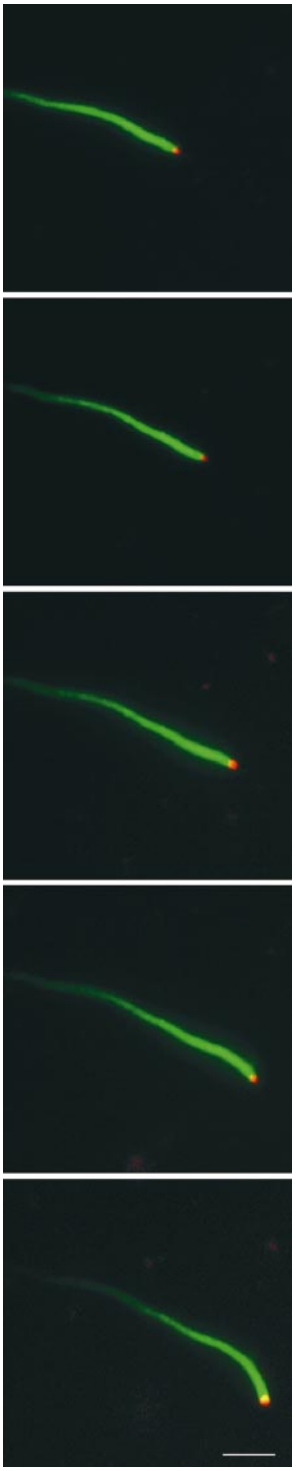

Figure 7. Actin-dependent propulsion of exogenous endosomes in *Xenopus* egg cytosol. HeLa cells were treated with Texas red transferrin (40 μg/ml) for 20 min at 37°C, and a postnuclear supernatant (PNS) was prepared. The PNS was diluted 60-fold with *Xenopus* egg cytosol containing 0.5 μM Alexa(488)-actin and 1 μM PMA. Alexa(488) and Texas red epifluorescence images were acquired every 10 s. Approximately half of the vesicles associated with actin comet tails contained internalized Texas red transferrin. Bar, 5 μm.

a vesicle motility reaction that was fixed in a flow chamber and visualized by immunolabeling with antibodies against Sec61β, an endoplasmic reticulum marker (Gorlich et al., 1992), along with FITC-phalloidin. Despite their abundance, Sec61β-positive membranes were never observed in association with actin comet tails (Fig. 8, A and E). Consistent with this observation, ER microsomes purified from canine pancreas failed to form actin comets (data not shown).

In a parallel experiment, early and recycling endosomes were labeled by allowing HeLa cells to internalize Texas red transferrin for 20 min. Quantitation of vesicle motility reactions indicated that 42% of the comet tails (n = 456) were associated with transferrin-positive vesicles (Fig. 8, B and E). To address the possibility that plasma membranes are partly responsible for the actin comet tails, cells were labeled at 4°C, a temperature at which endocytosis is blocked. Transferrin positive plasma membranes were an abundant constituent of the crude membranes in accord with previous observations (Sheff et al., 1999), yet they colocalized with only 1.4% of the comet tails (n = 433, Fig. 8, C and E). Finally, we found that nearly half of the actin comet tails (48%, n = 678) were associated with vesicles that stained intensely with a monoclonal antibody against human Lamp-1, a marker for late endosomes and lysosomes (Fig. 8, D and E). Internalized transferrin and Lamp-1 are thought to be largely nonoverlapping markers for the early/recycling and late endocytic pathways, respectively (Futter et al., 1996). We conclude that PMA-stimulated actin assembly occurs preferentially on the surface of endosomes and lysosomes. We note that in the absence of PMA, low levels of actin comet tails are generated constitutively by an as yet unidentified subpopulation of HeLa membranes.

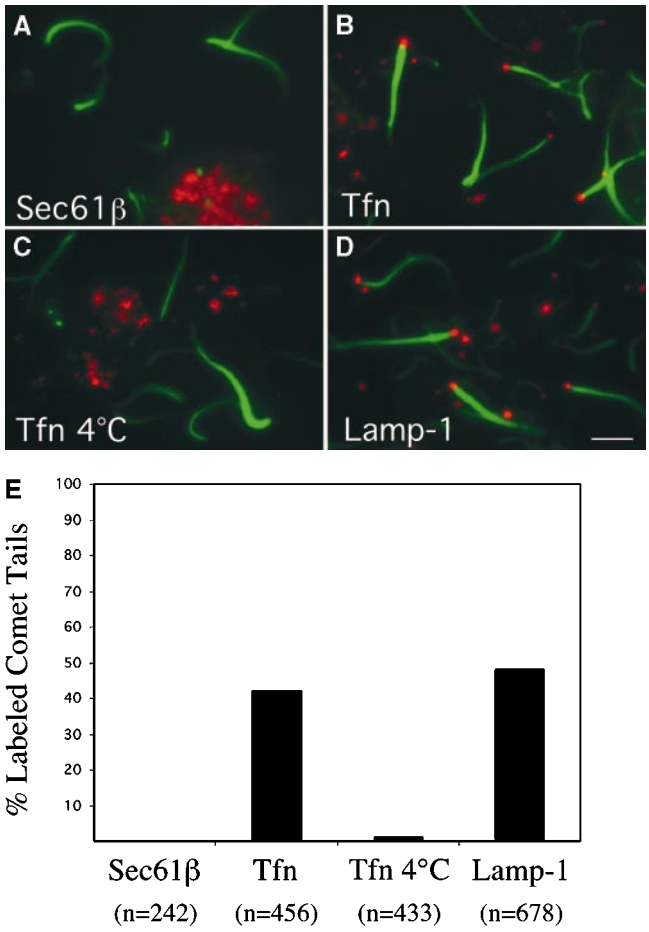

Figure 8. Endosomes and lysosomes preferentially nucleate actin assembly and move in vitro. HeLa postnuclear supernatants were prepared identically from unlabeled cells (A and D) and cells that had been treated with Texas red transferrin at 37°C (B) or 4°C (C). Cell-free motility reactions were fixed and processed for epifluorescence detection of organelle markers (red). F-actin (green, A–D) was detected with FITC-phalloidin. (A) ER membranes were immunodetected with affinity-purified anti-Sec61β antibodies followed by Texas red secondary antibodies. (B) Early and recycling endosomes were detected by labeling cells with Texas red transferrin for 20 min at 37°C. (C) Plasma membranes were detected by labeling cells with Texas red transferrin for 20 min at 4°C. (D) Lysosomes were immunodetected with anti–Lamp-1 H4A3 mAb followed by Texas red secondary antibodies. Bar, 5 μm. (E) Quantitation of comet tails associated with a labeled vesicle in the experiments described in A–D. The *n* value refers to the total number of actin comet tails counted under each condition from 8–10 random fields.

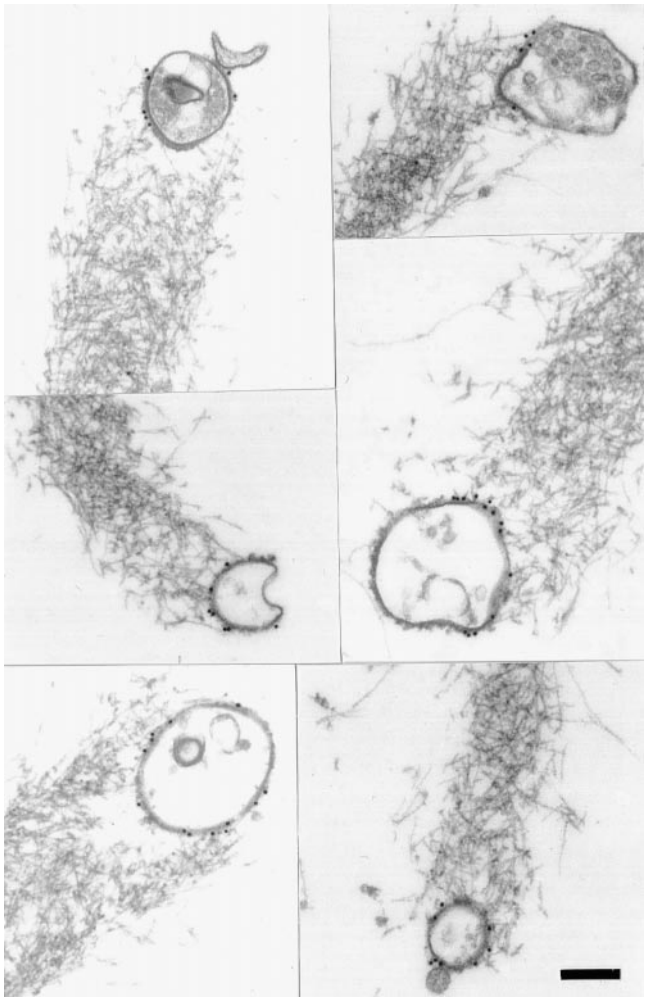

Figure 9. Gallery of electron micrographs depicting N-WASP immunogold-labeled HeLa vesicles associated with actin comet tails. Cell-free motility reactions containing unlabeled HeLa membranes were fixed in perfusion chambers, immunolabeled with affinity-purified N-WASP antibodies followed by 15 nm protein A–gold, and processed for electron microscopy. Gold particles are occasionally visible in the comet tails, but the vast majority are associated with the membrane. Note the similarity in vesicle morphology to the *Xenopus* egg vesicles shown in Fig. 6. Bar, 200 nm.

Actin nucleation by HeLa membranes in *Xenopus* cytosol was abolished by ToxB, and we confirmed by immunofluorescence analysis that N-WASP was recruited specifically to vesicles associated with actin comet tails (data not shown). Using the crude HeLa membranes as in Fig. 8, we examined the localization of N-WASP by immunoelectron microscopy (Fig. 9). Consistent with the results presented in Fig. 4, we observed N-WASP localization to the surface of every vesicle that was associated with an actin comet tail. Three additional features were revealed by this experiment. First, almost every gold particle was intimately associated with the vesicle membrane. Second, in most cases, the gold particles appeared to be distributed asymmetrically and were localized to the region of the vesicle contacting the actin comet tail. Third, the morphologies of the HeLa vesicles associated with actin comet tails, including crescent shapes and multivesicular lumens, were strikingly reminiscent of the *Xenopus* vesicles (Fig. 6).

Discussion

This work describes a relatively unexplored mode of intracellular vesicle movement. Propulsive movement is driven by actin assembly that is spatially restricted to the membrane-cytosol interface. Intracellular vesicles thus exploit a mechanism for movement that until recently was thought to be the exclusive purview of pathogenic micro-

organisms. In contrast to the rocketing movement of *Listeria* and *Shigella*, which is thought to be essential for cell to cell spreading, the reasons behind the sudden appearance of rocketing vesicles after Xenopus egg fertilization are unclear. The phenomenon temporally coincides with a massive increase in membrane flux induced by fertilization, but whether rocketing behavior plays a role in membrane trafficking is not yet known. Calcium-dependent cortical granule exocytosis, which is triggered by fertilization, is thought to be followed by a wave of membrane retrieval, and studies in sea urchin eggs have demonstrated that the exocytosis/endocytosis cycle induced by fertilization is mechanistically related to membrane recycling events in neuroendocrine cells and synaptic junctions (Conner and Wessel, 1998; Whalley et al., 1995). However, it is unlikely that all of the motile vesicles we observe correspond to newly recycled exocytic membranes as the actin comet tails did not colocalize with a fluid phase endocytic tracer introduced just before fertilization (our unpublished results). The motile vesicles may comprise a preexisting endosomal compartment that excludes endocytic vesicles formed as a result of cortical granule exocytosis.

The conditions under which rocketing vesicles were observed in *Xenopus* eggs are known to induce diacylglycerol synthesis and PKC activation (Stith et al., 1997). Although we lack definitive proof, several pieces of evidence suggest that PKC, or at least a protein that is similarly activated by diacylglycerol, plays a role in vesicle rocketing. First, in activated eggs actin comet tails were associated with vesicles that were enriched in GFP-XPKCα. Importantly, actin comets were also observed in naturally fertilized eggs, indicating that they are not an artifact of prick activation, GFP-XPKCα expression, or rhodamine-actin microinjection. Second, actin comet tails appeared during a time window that correlates with increased diacylglycerol production (Stith et al., 1997). Third, PMA, a high affinity ligand for the diacylglycerol activation domain of PKC, stimulated actin assembly-dependent vesicle movement in vivo and in vitro. Fourth, the PKC inhibitor BIM-I inhibited vesicle movement in vitro.

What are the downstream effects of PMA stimulation that ultimately lead to vesicle propulsion? We demonstrated that PMA stimulates the recruitment of N-WASP specifically to the surface of motile vesicles, as shown by immunofluorescence and immunogold labeling of cell-free motility reactions. The immunogold experiment reveals an intimate association between N-WASP and the membrane. Actin filaments in the comet tail are also associated with the membrane. In agreement with the mechanistic studies of *Shigella* movement by Egile et al. (1999), we hypothesize that associations between the actin comet tail and the vesicle membrane are mediated by the NH_2-terminal F-actin binding domain of N-WASP. The fact that latrunculin A inhibited comet tail formation without affecting N-WASP recruitment shows that these two subprocesses can be uncoupled from one another. This mechanistic feature is reminiscent of *Shigella*-mediated actin assembly wherein the *Shigella* outer membrane protein, IcsA, forms a high affinity complex with cytosolic N-WASP (Egile et al., 1999; Suzuki et al., 1998). Whereas *Shigella* movement does not require Rho GTPases (Mounier et al., 1999), N-WASP recruitment to vesicles was abolished by the *Clostridium difficile* toxin ToxB, an irreversible inhibitor of Rho family GTPases. This result provides circumstantial evidence for the involvement of Cdc42, since it is the only Rho family member that has been shown conclusively to activate N-WASP (Miki et al., 1998; Symons et al., 1996). An essential role for Cdc42 is also indicated by our unpublished result that pure, recombinant Cdc42/Rho-GDI complex rescues ToxB-mediated inhibition (manuscript in preparation). N-WASP interacts with Cdc42 only when it is bound to GTP (Miki et al., 1998). Thus, our data are consistent with a primary role for PMA in promoting the membrane recruitment of GTP-bound Cdc42, possibly via PKC-mediated phosphorylation of a membrane-associated nucleotide exchange factor. GTP-bound Cdc42 is then able to recruit and activate N-WASP. In solution, N-WASP is thought to exist in an autoinhibited conformation involving an intramolecular interaction between its Cdc42 interaction domain, and its COOH-terminal domain (Miki et al., 1998). Based on pyrene actin assembly assays with synthetic liposomes, it has been proposed that interactions between membrane phosphoinositides and the N-WASP PH domain, in concert with GTP-bound Cdc42, mediate allosteric activation of N-WASP (Rohatgi et al., 1999). It will be interesting to test this hypothesis with biological membranes and recombinant N-WASP constructs using the functional and morphological assays described in this paper.

What is the identity of the moving vesicles? Our data suggest that the majority of actin comet tails are associated with endosomes and lysosomes. First, motile vesicles from *Xenopus* eggs accumulate the weakly basic dye acridine orange in a bafilomycin-sensitive manner, indicating that they belong to an acidic subcellular compartment. Second, ultrastructural examination of the motile vesicles revealed highly irregular, multivesicular profiles consistent with an endosomal morphology (Wall and Patel, 1987). Third, HeLa cell endosomes containing internalized transferrin nucleated actin assembly and moved as efficiently as the *Xenopus* egg vesicles when added to *Xenopus* cytosol. Fourth, using crude HeLa cell membranes, we determined that the majority of the actin comet tails were associated with early/recycling endosomes (transferrin positive) and late endosomes/lysosomes (Lamp-1 positive). Finally, membrane specificity is evident from our observation that neither mitochondria nor Sec61 positive ER membranes ever assembled actin comet tails. Although endosomes and lysosomes accounted for the vast majority of the vesicles associated with actin comet tails in our system, other organelles might be able to nucleate actin assembly. It is possible that the potent activating effects of PMA bias the recruitment of limiting components of the signaling (e.g., Cdc42) and actin nucleation machinery (e.g., N-WASP) to membranes enriched in PKC-dependent signaling components, for example. We have not ruled out the possibility that membranes derived from the secretory pathway also nucleate actin assembly. The demonstration that overexpressed dominant alleles of Cdc42 interfere with aspects of Golgi trafficking in polarized epithelial cells is consistent with this possibility (Kroschewski et al., 1999).

What function does actin-based vesicle propulsion serve, especially given its apparently random direction? Pinosomes, which are functionally distinct from endosomes

and lysosomes, have been observed at the tips of dynamic actin comet tails in mast cells and macrophages cultured in hyperosmolar media or after treatment with Ni^{2+} or La^{3+}, respectively (Heuser and Morisaki, 1992; Merrifield et al., 1999). In a recent report, Merrifield et al. (1999) proposed a model wherein actin assembly on the surface of a nascent pinosome is intimately tied to the pinocytic event which is initiated by a burst of actin assembly at the plasma membrane. As the newly formed endosome pinches off, it is propelled away from the plasma membrane by sustained actin assembly on its surface. We propose to extend this model to incorporate extant endosomes, lysosomes, and possibly other organelles. In this model, the transient accumulation of signaling lipids (e.g., diacylglycerol) on the membrane recruits cytosolic actin nucleation factors as a means of pushing the endosome through the cytoplasm. Actin-based propulsion of endosomes and lysosomes may be a rare and transient event in most cell types, especially in the more two-dimensional cells whose cytoskeletons are easiest to visualize. The force provided by actin assembly may enhance the efficiency of organelle movement, especially in a large three-dimensional cell such as the *Xenopus* egg. Microtubule tracks, which provide directed transport of endosomes and lysosomes over long distances, may not adequately cover three-dimensional space, despite their dynamicity. Nondirected vesicle propulsion, which may be seen as a form of ATP-dependent diffusion, may work in concert with microtubule capture to move large particles through the crowded and bustling cytoplasmic milieu.

A role for actin filaments in maintaining the steady-state distribution of endosomes and lysosomes as well as coordinating membrane traffic between these compartments has been implicated in several experimental systems. Cytochalasin D, which inhibits actin filament assembly, has been found to impair the delivery of cargo from late endosomes to lysosomes and to disrupt the organization of endosomes in certain cell lines (van Deurs et al., 1995; Barois et al., 1998). In addition, jasplakinolide, a toxin that stabilizes actin filaments and inhibits filament disassembly, causes the accumulation of internalized fluid phase markers in a late endosomal compartment of polarized epithelial cells (Shurety et al., 1998). Involvement of actin dynamics in the steady-state positioning of late endosomes and lysosomes is also suggested by phenotypic analysis of cells deficient in the actin cross-linking protein, filamin (Liu et al., 1997). In the mutant cells, late endosomes are dispersed throughout the cytoplasm, whereas in a matched cell line expressing filamin they are clustered around the nucleus. The mechanisms underlying these observations have not been elucidated, but may relate to the ability of intracellular membranes to nucleate actin assembly, as described in this paper.

The most obvious function for actin nucleation by endosomes and lysosomes is in their physical movement, but there may also be functional implications for the actin cytoskeleton. We do not know how the majority of actin filaments in the cell are generated or positioned. The leading edge of a motile cell is a major nucleation site, but probably cannot account for all the filaments in a large cell. We speculate that intracellular membranes, via N-WASP and the Arp2/3 complex, may nucleate the assembly of actin filaments which are then organized into networks by myosins, bundlers, and cross-linkers.

We are especially grateful to Marc Kirschner for providing antibodies against N-WASP. We also thank Tom Rapoport for anti-Sec61β antibodies, Fred Hofmann and Klaus Aktories for the GST-ToxB expression plasmid, Bill Brieher for Alexa(488)-labeled actin, Zach Perlman for help with data analysis, and Bill Brieher, Mimi Shirasu, Jennifer Tirnauer, and Rebecca Ward for critiquing the manuscript.

This work was supported by a Life Sciences Research Foundation fellowship to J.T. (Amgen fellow), a National Institutes of Health grant (GM35126) to T.J. Mitchison and a US Department of Defense/Breast Cancer Research Program grant (no. B696-337) to C.A. Larabell. Support was also provided by the Office of Health and Environmental Research of the US Department of Energy (contract no. DE-AC03-SF00098). R.T. Moon acknowledges support as an Investigator of the Howard Hughes Medical Institute.

Submitted: 13 August 1999
Revised: 7 December 1999
Accepted: 20 December 1999

References

Barois, N., F. Forquet, and J. Davoust. 1998. Actin microfilaments control the MHC class II antigen presentation pathway in B cells. *J. Cell Sci.* 111:1791–1800.

Bement, W.M., and D.G. Capco. 1989. Activators of protein kinase C trigger cortical granule exocytosis, cortical contraction, and cleavage furrow formation in *Xenopus laevis* oocytes and eggs. *J. Cell Biol.* 108:885–892.

Bement, W.M., and D.G. Capco. 1991. Parallel pathways of cell cycle control during *Xenopus* egg activation. *Proc. Natl. Acad. Sci. USA*. 88:5172–5176.

Boyles, J., L. Anderson, and P. Hutcherson. 1985. A new fixative for the preservation of actin filaments: fixation of pure actin filament pellets. *J. Histochem. Cytochem*. 33:1116–1128.

Chen, K.H., Z.G. Peng, S. Lavu, and H.F. Kung. 1988. Molecular cloning and sequence analysis of two distinct types of *Xenopus* laevis protein kinase C. *Second Messengers Phosphoproteins.* 12:251–260.

Conner, S., and G.M. Wessel. 1998. Rab3 mediates cortical granule exocytosis in the sea urchin egg. *Dev. Biol.* 203:334–344.

Egile, C., T.P. Loisel, V. Laurent, R. Li, D. Pantaloni, P.J. Sansonetti, and M.F. Carlier. 1999. Activation of the CDC42 effector N-WASP by the *Shigella flexneri* IcsA protein promotes actin nucleation by Arp2/3 complex and bacterial actin-based motility. *J. Cell Biol.* 146:1319–1332.

Futter, C.E., A. Pearse, L.J. Hewlett, and C.R. Hopkins. 1996. Multivesicular endosomes containing internalized EGF-EGF receptor complexes mature and then fuse directly with lysosomes. *J. Cell Biol.* 132:1011–1023.

Goodson, H.V., C. Valetti, and T.E. Kreis. 1997. Motors and membrane traffic. *Curr. Opin. Cell Biol.* 9:18–28.

Gorlich, D., S. Prehn, E. Hartmann, K.U. Kalies, and T.A. Rapoport. 1992. A mammalian homolog of SEC61p and SECYp is associated with ribosomes and nascent polypeptides during translocation. *Cell*. 71:489–503.

Heim, R., A.B. Cubitt, and R.Y. Tsien. 1995. Improved green fluorescence. *Nature*. 373:663–664.

Heuser, J.E., and J.H. Morisaki. 1992. Time-lapse video microscopy of endosomal "rocketing" in La/Zn treated cells. *Mol Biol. Cell Abstr.* 3:172.

Higley, S., and M. Way. 1997. Actin and cell pathogenesis. *Curr. Opin. Cell Biol.* 9:62–69.

Hofmann, F., C. Busch, U. Prepens, I. Just, and K. Aktories. 1997. Localization of the glucosyltransferase activity of *Clostridium difficile* toxin B to the N-terminal part of the holotoxin. *J. Biol. Chem.* 272:11074–11078.

Kellogg, D.R., T.J. Mitchison, and B.M. Alberts. 1988. Behaviour of microtubules and actin filaments in living *Drosophila* embryos. *Development*. 103: 675–686.

Kroschewski, R., A. Hall, and I. Mellman. 1999. Cdc42 controls secretory and endocytic transport to the basolateral plasma membrane of MDCK cells. *Nat. Cell Biol.* 1:8–13.

Larabell, C. 1999. Confocal microscopy of live *Xenopus* eggs, oocytes, and embryos. *Methods Mol. Biol.* In press.

Liu, G., L. Thomas, R.A. Warren, C.A. Enns, C.C. Cunningham, J.H. Hartwig, and G. Thomas. 1997. Cytoskeletal protein ABP-280 directs the intracellular trafficking of furin and modulates proprotein processing in the endocytic pathway. *J. Cell Biol.* 139:1719–1733.

Loisel, T.P., R. Boujemaa, D. Pantaloni, and M.F. Carlier. 1999. Reconstitution of actin-based motility of *Listeria* and *Shigella* using pure proteins. *Nature*. 401:613–616.

Ma, L., L.C. Cantley, P.A. Janmey, and M.W. Kirschner. 1998. Corequirement of specific phosphoinositides and small GTP-binding protein Cdc42 in inducing actin assembly in *Xenopus* egg extracts. *J. Cell Biol.* 140:1125–1136.

Marchand, J.B., P. Moreau, A. Paoletti, P. Cossart, M.F. Carlier, and D. Panta-

loni. 1995. Actin-based movement of *Listeria monocytogenes*: actin assembly results from the local maintenance of uncapped filament barbed ends at the bacterium surface. *J. Cell Biol.* 130:331–343.
Matteoni, R., and T.E. Kreis. 1987. Translocation and clustering of endosomes and lysosomes depends on microtubules. *J. Cell Biol.* 105:1253–1265.
Merrifield, C.J., S.E. Moss, C. Ballestrem, B.A. Imhof, G. Giesc, I. Wunderlich, and W. Almers. 1999. Endocytic vesicles move at the tips of actin tails in cultured mast cells. *Nature Cell Biol.* 1:72–74.
Miki, H., T. Sasaki, Y. Takai, and T. Takenawa. 1998. Induction of filopodium formation by a WASP-related actin-depolymerizing protein N-WASP. *Nature*. 391:93–96.
Moreau, V., and M. Way. 1998. Cdc42 is required for membrane dependent actin polymerization in vitro. *FEBS Lett.* 427:353–356.
Mounier, J., V. Laurent, A. Hall, P. Fort, M.F. Carlier, P.J. Sansonetti, and C. Egile. 1999. Rho family GTPases control entry of *Shigella flexneri* into epithelial cells but not intracellular motility. *J. Cell Sci.* 112:2069–2080.
Murray, A.W., and M.W. Kirschner. 1989. Cyclin synthesis drives the early embryonic cell cycle. *Nature*. 339:275–280.
Rohatgi, R., L. Ma, H. Miki, M. Lopez, T. Kirchhausen, T. Takenawa, and M.W. Kirschner. 1999. The interaction between N-WASP and the Arp2/3 complex links Cdc42-dependent signals to actin assembly. *Cell*. 97:221–231.
Rowning, B.A., J. Wells, M. Wu, J.C. Gerhart, R.T. Moon, and C.A. Larabell. 1997. Microtubule-mediated transport of organelles and localization beta-catenin to the future dorsal side of *Xenopus* eggs. *Proc. Natl. Acad. Sci. USA*. 94:1224–1229.
Sheff, D.R., E.A. Daro, M. Hull, and I. Mellman. 1999. The recycling pathway contains two distinct populations of early endosomes with different sorting functions. *J. Cell Biol.* 145:123–139.
Sheldahl, L.C., M. Park, C.C. Malbon, and R.T. Moon. 1999. Protein kinase C is differently stimulated by Wnt and Frizzled homologs in a G-protein-dependent manner. *Curr. Biol.* 9:695–698.
Shurety, W., N.L. Stewart, and J.L. Stow. 1998. Fluid-phase markers in the basolateral endocytic pathway accumulate in response to the actin assembly-promoting drug jasplakinolide. *Mol. Biol. Cell.* 9:957–975.
Stith, B.J., K. Woronoff, R. Espinoza, and T. Smart. 1997. sn-1,2-diacylglycerol and choline increase after fertilization in *Xenopus laevis*. *Mol. Biol. Cell.* 8:755–765.
Suzuki, T., H. Miki, T. Takenawa, and C. Sasakawa. 1998. Neural Wiskott-Aldrich syndrome protein is implicated in the actin-based motility of *Shigella flexneri*. *EMBO (Eur. Mol. Biol. Organ.) J.* 17:2767–2776.
Symons, M., J.M. Derry, B. Karlak, S. Jiang, V. Lemahieu, F. McCormick, U. Francke, and A. Abo. 1996. Wiskott-Aldrich syndrome protein, a novel effector for the GTPase CDC42Hs, is implicated in actin polymerization. *Cell*. 84:723–734.
Toullec, D., P. Pianetti, H. Coste, P. Bellevergue, T. Grand-Perret, M. Ajakane, V. Baudet, P. Boissin, E. Boursier, F. Loriolle, et al. 1991. The bisindolylmaleimide GF 109203X is a potent and selective inhibitor of protein kinase C. *J. Biol. Chem*. 266:15771–15781.
van Deurs, B., P.K. Holm, L. Kayser, and K. Sandvig. 1995. Delivery to lysosomes in the human carcinoma cell line HEp-2 involves an actin filament-facilitated fusion between mature endosomes and preexisting lysosomes. *Eur. J. Cell Biol.* 66:309–323.
Wall, D.A., and S. Patel. 1987. Multivesicular bodies play a key role in vitellogenin endocytosis by *Xenopus* oocytes. *Dev. Biol.* 119:275–289.
Whalley, T., M. Terasaki, M.S. Cho, and S.S. Vogel. 1995. Direct membrane retrieval into large vesicles after exocytosis in sea urchin eggs. *J. Cell Biol.* 131: 1183–1192.